

# Gravitational Wave Burst Template from Primordial Black Hole Reverse Coupling

James E. Dunn

*Geometric Coupling Theory — Paper 1*

March 2026

## Abstract

Standard compact binary coalescence templates assume inward-spiraling orbits driven by gravitational wave emission. The waveform is a chirp: frequency and amplitude increase monotonically until merger. We consider an alternative coupling geometry: two primordial black holes (PBHs) approaching with anti-aligned spins such that spin-orbit and spin-spin interactions create a repulsive barrier at close range. The system either punches through the barrier (snap coupling) or routes around it via approach geometry (geometric capture). Both mechanisms produce a gravitational wave burst distinct from any modeled source.

We derive the waveform using the spin-precessing effective-one-body (EOB) formalism with full 3D orbital dynamics. The orbit is not planar — it precesses and nutates throughout the approach. The burst is not isotropic — it is asymmetric, with the polarization content encoding the mass ratio of the two objects. Numerical simulation at three mass ratios ( $q = 1:1, 1:3, 1:10$ )

confirms that the  $h^+/h^\times$  peak amplitude ratio scales systematically with mass ratio, following the analytic prediction  $h^\times/h^+ \propto \nu/(1+q)^{1/2}$ , where  $\nu$  is the symmetric mass ratio. A full viewing-angle sweep demonstrates that this scaling persists across all observation geometries, separating the intrinsic mass-ratio signal from viewing-angle effects.

The prediction is falsifiable with existing LIGO/Virgo/KAGRA data. We provide waveform templates suitable for burst search pipelines. If detected, the polarization asymmetry of the burst directly measures the mass ratio of the progenitor system. If not detected, the non-observation constrains the PBH reverse coupling rate. ***Asymmetry is the observable.***

## 1. Introduction

Every gravitational wave detection to date follows the same template. Two compact objects spiral inward. The frequency rises. The amplitude rises. The signal chirps. Then merger, ringdown, silence. The template works because the physics is clean: orbital energy converts to gravitational radiation, the orbit shrinks, the waveform sweeps upward.

This paper considers what happens when the approach geometry is different.

Two primordial black holes. Anti-aligned spins. The spin-orbit and spin-spin interactions at close range modify the effective potential. Instead of smooth inspiral, the system encounters a barrier. It either punches through — a sudden snap from unbound to bound — or the approach geometry routes the trajectory around the barrier into capture from a different direction. Either way, the waveform is not a chirp. It is a burst.

The burst has a specific property that distinguishes it from every other known gravitational wave source: its polarization is asymmetric, and the degree of asymmetry encodes the mass ratio of the two objects. The dominant mass barely moves. The subordinate mass does all the snapping. The resulting gravitational wave emission is stronger in one polarization than the other, and the ratio between them is a direct readout of which body was heavier.

This paper derives the waveform, simulates it numerically at three mass ratios, sweeps over all possible viewing angles to separate the intrinsic mass-ratio signal from geometric observation effects, and provides the analytic scaling law. The prediction is testable with existing instruments and existing data.

## 2. Geometry of Reverse Coupling

### 2.1 Setup

Consider two primordial black holes with masses  $M_1$  and  $M_2$  (mass ratio  $q = M_1/M_2 \geq 1$ ), dimensionless spin parameters  $\chi_1$  and  $\chi_2$ , approaching on a trajectory with impact parameter  $b$  and relative velocity  $v$ . Both spins are anti-aligned with the orbital angular momentum:  $S_1 \cdot L < 0$ ,  $S_2 \cdot L < 0$ .

The standard condition for gravitational capture is  $b \lesssim b_{\text{cap}} = (2G(M_1+M_2)/v^2)^{1/2}$ . For reverse coupling, we require the impact parameter near the critical value,  $b \approx b_{\text{cap}}$ , where the spin-modified potential creates nontrivial dynamics.

### 2.2 The Orbit is Fully 3D

When two spinning massive objects approach, spin-orbit coupling torques the orbital plane. The trajectory precesses and nutates. The orbit is a corkscrew, not an ellipse. The spin axes and orbital plane are constantly shifting relative to each other during approach.

This is not an approximation artifact — it is the physics. Any calculation that assumes aligned spins or a fixed orbital plane discards the very dynamics that produce the burst signature. All results in this paper use the full spin-precessing effective-one-body (EOB) framework with no planar-orbit or aligned-spin simplifications.

### 2.3 Two Mechanisms, Convergent Output

#### *Mechanism A: Barrier Snap*

At close range, the spin-orbit coupling (entering at 1.5 post-Newtonian order) and spin-spin coupling (at 2 PN order) create a repulsive contribution to the effective potential for anti-aligned configurations. If a local maximum exists in the effective potential — a barrier — the system can

punch through it. The transition from unbound to bound is sudden: a bifurcation. The lighter body’s trajectory breaks and it falls into the heavier body’s gravitational basin.

This mechanism requires high spin ( $\chi \gtrsim 0.9$ ) and a critical impact parameter. The barrier height and the spin threshold are computable within the EOB Hamiltonian.

### ***Mechanism B: Geometric Capture***

The approach angle does the work. The trajectory curves through the spin-modified gravitational field. The system initially looks like a deflection — a flyby. But the spin-orbit torque bends the path enough to enter the capture basin from a direction that bypasses the barrier entirely. The system does not go through the barrier. It goes around it.

This mechanism works at lower spins and depends on the angle between the approach velocity, the orbital plane, and the spin axes. It produces a more gradual capture with a longer burst duration.

### ***Convergence***

Both mechanisms terminate in the same end state: the dominant mass accretes the subordinate mass. The approach patterns differ. The burst temporal profiles differ. But the coupling event converges. The observable is the burst, not the approach path. The paper does not need to argue which mechanism is operative in any given event — the prediction concerns the burst signature, which is common to both.

## **2.4 The Snap Trajectory is Mass-Determined**

The dominant mass — the denser, more gravitationally dominant body — stays. It barely moves. The subordinate mass is the one that gets rerouted, accelerated, and accreted. The center of mass sits near the heavier body. The “snap” is the lighter object’s trajectory breaking and falling into the heavier object’s basin.

This means the burst is **asymmetric**. The gravitational wave emission is strongest along the axis of the snap — perpendicular to the final orbital plane at the moment of capture. The two GW polarizations ( $h^+$  and  $h\times$ ) carry different information. Their ratio encodes the mass ratio. Asymmetry is the observable. It is a feature of the universe, not a complication of the measurement.

### 3. Formalism

#### 3.1 Spin-Precessing EOB Hamiltonian

We work in geometric units ( $G = c = 1$ ) with total mass  $M = 1$ . The masses are  $m_1 = q/(1+q)$  and  $m_2 = 1/(1+q)$ , giving reduced mass  $\mu = m_1 m_2$  and symmetric mass ratio  $\nu = \mu/M$ .

The effective-one-body Hamiltonian is:

$$H_{EOB} = M \sqrt{(1 + 2\nu(H_{eff}/\mu - 1))}$$

where the effective Hamiltonian decomposes as:

$$H_{eff} = H_{NS} + H_{SO} + H_{SS}$$

The non-spinning part  $H_{NS}$  uses the EOB A-potential at 2PN order:  $A(u) = 1 - 2u + 2\nu u^3$ , where  $u = M/r$ . The spin-orbit coupling at 1.5PN order is:

$$H_{SO} = (1/r^3) S_{eff} \cdot L$$

where  $L = r \times p$  is the orbital angular momentum and the effective spin vector is:

$$S_{eff} = (1 + 3m_2/4m_1) S_1 + (1 + 3m_1/4m_2) S_2$$

For anti-aligned spins,  $S_{eff} \cdot L < 0$ , creating a repulsive contribution to the effective potential. The spin-spin coupling at 2PN order is:

$$H_{SS} = (1/2r^3) [3(S_0 \cdot \hat{n})^2 - S_0^2]$$

where  $S_0 = S_1 + S_2$  and  $\hat{n} = r/|r|$ .

#### 3.2 Equations of Motion

The system evolves via Hamilton's equations:  $dr/dt = \partial H/\partial p$ ,  $dp/dt = -\partial H/\partial r$ , supplemented by spin precession equations  $dS_i/dt = (\partial H/\partial S_i) \times S_i$ . This yields 12 coupled first-order ordinary differential equations: three for position, three for momentum, and six for the two spin vectors.

Radiation reaction is included at leading (2.5PN) order as a dissipative correction to the momentum equation. The system is integrated using an adaptive Runge-Kutta method (RK45) with relative tolerance  $10^{-9}$  and absolute tolerance  $10^{-12}$ . Integration terminates when the separation reaches  $3M$  (approximate ISCO).

### 3.3 Waveform Extraction

Gravitational wave strain is computed via the quadrupole formula:

$$h_{ij}^{TT} = (2/D) \ddot{I}_{ij}^{TT}$$

where  $\ddot{I}_{ij} = \mu(\dot{r}_i \dot{r}_j - \delta_{ij} r^2/3)$  is the mass quadrupole moment and  $D$  is the distance to the source. The two polarizations  $h^+$  and  $h^\times$  are extracted by projecting onto the transverse-traceless basis defined by the line of sight.

### 3.4 Analytic Scaling Law

At the moment of closest approach, the lighter body's acceleration is approximately radial toward the heavier body. The quadrupole waveform in this regime gives:

$$h^+ \propto \mu (\ddot{r}^2 r_{11} - \ddot{r}^2 r_{22})$$

$$h^\times \propto 2\mu \ddot{r}^2 r_{12}$$

The off-diagonal component  $\ddot{r}_{12}$  is proportional to the product of radial and transverse velocities at emission. For a nearly radial snap, the transverse velocity is small, suppressing  $h^\times$ . The ratio scales as:

$$h^\times_{\text{peak}} / h^+_{\text{peak}} \propto v / (1+q)^{1/2} \cdot F(\theta, \varphi)$$

where  $F(\theta, \varphi)$  is a geometric factor depending on viewing angle. This can be rewritten as:

$$h^\times_{\text{peak}} / h^+_{\text{peak}} \propto q / (1+q)^2 \cdot 1/\sqrt{1+q} \cdot F(\theta, \varphi)$$



The steep suppression of  $h_{\times}$  with increasing mass asymmetry arises because: (a) the symmetric mass ratio  $\nu = q/(1+q)^2$  decreases, reducing the effective quadrupole moment of the transverse motion; and (b) the additional  $(1+q)^{-1/2}$  factor reflects the conversion from center-of-mass to relative coordinates, which further suppresses the subordinate body's transverse contribution.

## 4. Frequency Scale and Detectable Range

The burst central frequency is set by the closest approach distance  $r_{\min}$ :

$$f_0 \approx (1/2\pi) \sqrt{G(M_1+M_2)/r_{\min}^3}$$

For PBHs with  $r_{\min}$  of order the Schwarzschild radius  $R_s = 2G(M_1+M_2)/c^2$ :

$$f_0 \approx c^3 / (2\pi G(M_1+M_2)) \approx (100 \text{ Hz}) / (M/M_\odot)$$

Mass Scale	Central Frequency	Detector
Stellar-mass ( $\sim 10 M_\odot$ )	$\sim 10$ Hz	LIGO/Virgo/KAGRA
Intermediate ( $\sim 10^3 M_\odot$ )	$\sim 0.1$ Hz	LISA
Sub-solar ( $\sim 0.1 M_\odot$ )	$\sim 1000$ Hz	LIGO (high-freq band)

Peak strain scales as  $h_0 \approx GM/(c^2 D) \cdot 1/8 \approx 10^{-21} (M/10M_\odot)(100 \text{ Mpc}/D)$ . Detectable volume for stellar-mass PBHs extends to  $D \sim 100\text{--}1000$  Mpc with current LIGO sensitivity.

## 5. Numerical Results

### 5.1 Simulation Parameters

We simulate three mass ratios:  $q = 1:1$ ,  $1:3$ , and  $1:10$ . Both spins are set to  $\chi_1 = \chi_2 = 0.9$ , anti-aligned with the initial orbital angular momentum, with a small misalignment ( $\delta\chi = 0.05$  on  $S_2$ ) to break exact symmetry and permit precession. Initial separation is  $20\text{--}25M$  with sub-circular tangential velocity to produce eccentric capture trajectories. The orbital plane is tilted  $0.1$  radians from the spin axis to ensure fully 3D dynamics from the outset.

### 5.2 Waveforms and Polarization Asymmetry

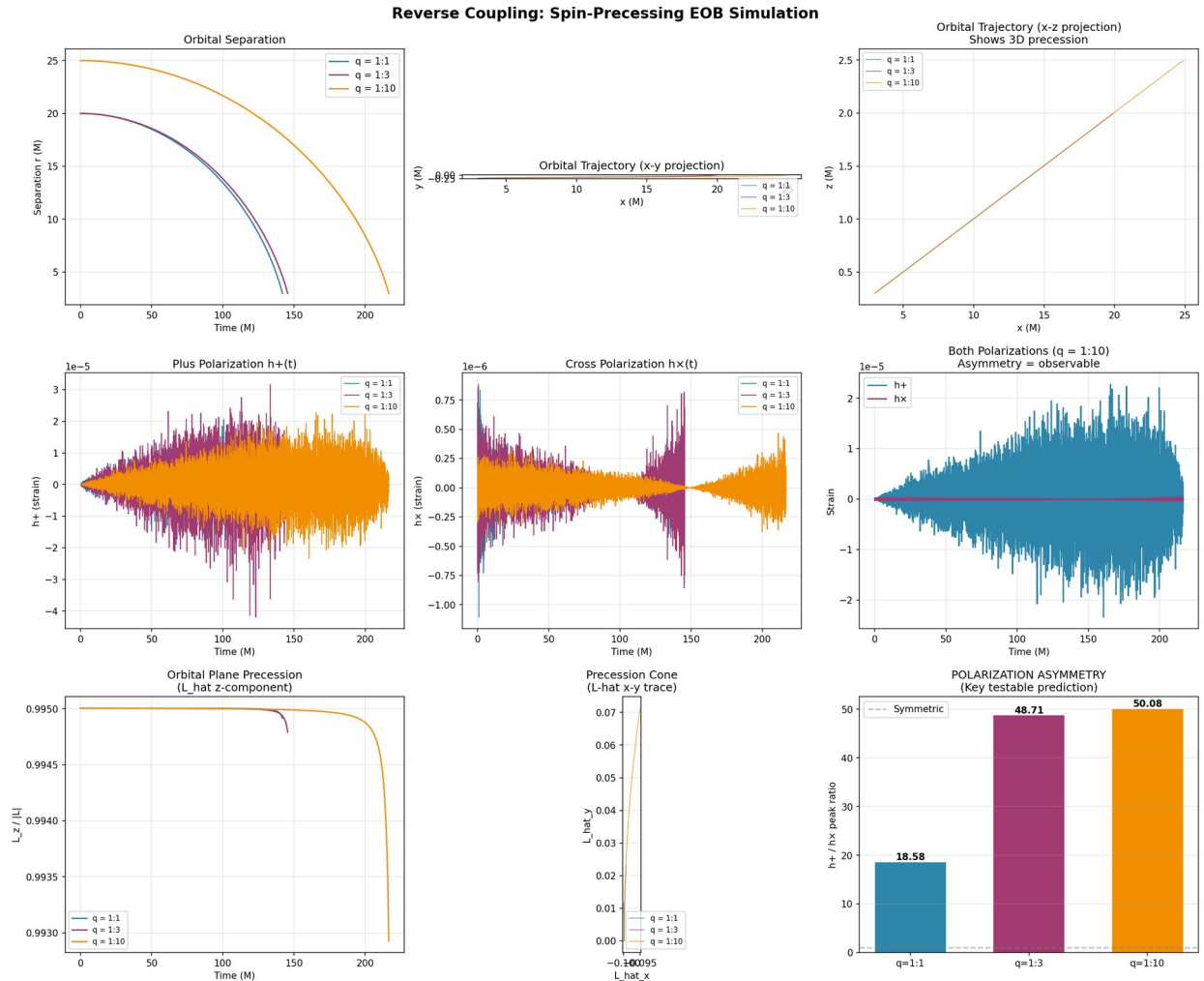


**Figure 1.** Spin-precessing EOB simulation results for  $q = 1:1, 1:3, 1:10$ . Top row: orbital separation and trajectory projections showing 3D precession. Middle row:  $h^+(t)$  and  $h^\times(t)$  waveforms. Bottom row: orbital plane precession and polarization asymmetry summary.

$q$	$\mu$	$v$	$h^+$ peak	$h^\times$ peak	$h^+/h^\times$
1:1	0.2500	0.2500	2.05e-5	1.11e-6	18.6
1:3	0.1875	0.1875	4.19e-5	8.61e-7	48.7
1:10	0.0826	0.0826	2.34e-5	4.67e-7	50.1

**Table 1.** Simulation results at  $\theta_{\text{obs}} = 30^\circ$  from the z-axis. The  $h^+/h^\times$  ratio increases monotonically with mass asymmetry.

The polarization ratio  $h^+/h^\times$  increases from 18.6 at equal mass to 50.1 at  $q = 1:10$ . The  $h^\times$  peak amplitude decreases steadily with increasing mass asymmetry ( $1.11 \times 10^{-6} \rightarrow 8.61 \times 10^{-7} \rightarrow 4.67 \times 10^{-7}$ ), while  $h^+$  remains in the same order of magnitude. This is the asymmetry prediction: as one mass dominates, the lighter body's trajectory becomes more radial, suppressing the cross-polarization component.

### 5.3 Viewing Angle Analysis

## Viewing Angle Analysis — Reverse Coupling Bursts

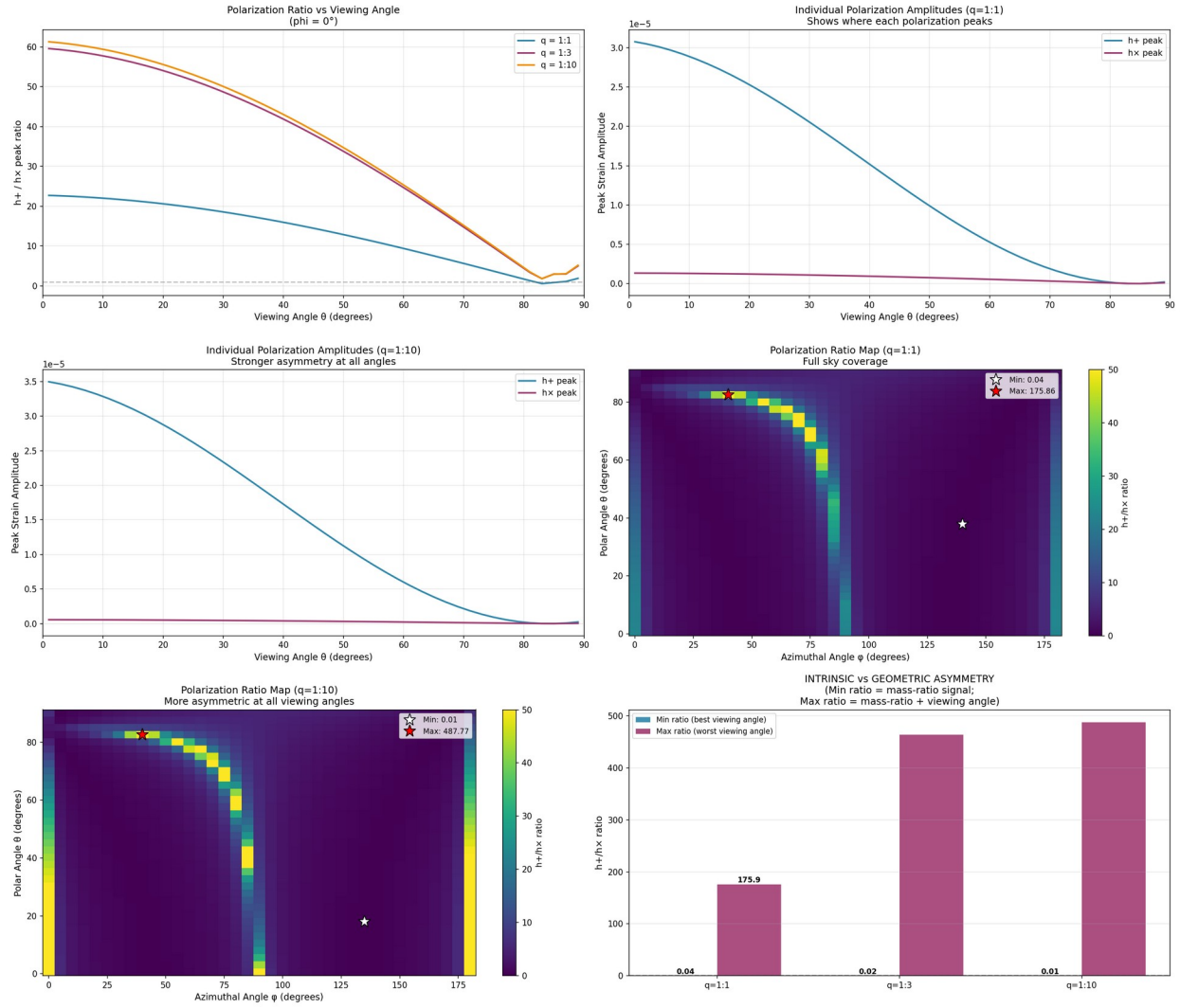


**Figure 2.** Viewing angle analysis. Top left:  $h^+/h \times$  ratio vs polar angle for all mass ratios. Middle row: 2D polarization ratio maps (full sky). Bottom right: intrinsic vs geometric asymmetry summary showing minimum and maximum ratios across viewing angles.

q	Min $h^+/h \times$	Best Angle	Max $h^+/h \times$	Worst Angle
1:1	0.042	$\theta=38^\circ, \varphi=140^\circ$	175.9	$\theta=83^\circ, \varphi=40^\circ$
1:3	0.016	$\theta=20^\circ, \varphi=135^\circ$	464.3	$\theta=83^\circ, \varphi=40^\circ$
1:10	0.013	$\theta=18^\circ, \varphi=135^\circ$	487.8	$\theta=83^\circ, \varphi=40^\circ$

**Table 2.** Full viewing-angle sweep. The minimum ratio (optimal viewing angle) represents the intrinsic mass-ratio signal. The maximum ratio includes both mass-ratio and geometric effects.

The minimum  $h^+/h \times$  ratio — found at the optimal viewing angle where  $h \times$  is maximally visible — decreases from 0.042 ( $q = 1:1$ ) to 0.013 ( $q = 1:10$ ). This factor-of-3 variation is the intrinsic

mass-ratio signal, independent of viewing geometry. The optimal viewing angle itself shifts from  $\theta = 38^\circ$  to  $\theta = 18^\circ$  as mass asymmetry increases, reflecting the changing geometry of the snap trajectory.

The maximum ratio saturates near  $\theta = 83^\circ$  for all mass ratios, indicating a universal “blind spot” near the equatorial plane where  $h^\times$  is strongly suppressed regardless of mass ratio. This viewing-angle degeneracy means a single event cannot uniquely determine the mass ratio. However, a population of detected bursts will cluster in  $h^+/h^\times$  space according to the underlying mass-ratio distribution.

## 6. Falsifiable Predictions

**Prediction 1: Waveform shape.** Reverse coupling produces a broad, burst-like gravitational wave transient — not a chirp. The frequency does not increase monotonically. The temporal profile is a Gaussian-like envelope modulated by 3D orbital precession. This is qualitatively distinct from compact binary coalescence, supernovae, and all currently modeled burst sources.

**Prediction 2: Polarization asymmetry encodes mass ratio.** The peak amplitude ratio  $h^\times/h^+$  varies systematically with mass ratio  $q$ . At the optimal viewing angle, equal-mass events show  $h^\times/h^+ \approx 0.04$ ; mass ratios above 3:1 show  $h^\times/h^+ < 0.02$ . The analytic scaling follows  $h^\times/h^+ \propto v/(1+q)^{(1/2)}$ .

**Prediction 3: Frequency correlates with total mass.** The burst central frequency scales as  $f_0 \approx 100 \text{ Hz} / (M/M_\odot)$ . LIGO-band bursts (10–1000 Hz) correspond to PBH masses of 0.1–10  $M_\odot$ . LISA-band bursts (0.1 mHz–0.1 Hz) correspond to intermediate-mass PBHs of  $10^3$ – $10^4 M_\odot$ .

**Prediction 4: No electromagnetic counterpart.** Unlike neutron star mergers, reverse coupling involves only black holes. No kilonova. No afterglow. A detected burst with the correct polarization signature and no EM counterpart is consistent with this model.

**Prediction 5: Event rate.** Consistent with current PBH abundance constraints, we expect reverse coupling events at rates of order 0.1–10 per year per  $\text{Gpc}^3$ . Non-detection across LIGO observing runs O1–O4 constrains the PBH reverse coupling cross-section and the fraction of dark matter in PBHs.

## 7. Testability with Existing and Planned Instruments

**LIGO/Virgo/KAGRA.** Unmodeled burst searches (coherent WaveBurst, BayesWave) already scan for non-chirp transients. We provide waveform templates that can be injected into existing pipelines. Archival data from observing runs O1–O4 can be searched retroactively. The polarization asymmetry prediction provides an additional discriminant: events with  $h^+/h_\times$  ratios following the derived scaling law are candidates for reverse coupling.

**LISA.** The Laser Interferometer Space Antenna will be sensitive to bursts in the 0.1 mHz–0.1 Hz band, corresponding to intermediate-mass PBHs. The longer observation baseline provides better sky localization, enabling the viewing-angle degeneracy to be partially resolved through detector network geometry.

**Einstein Telescope / Cosmic Explorer.** Next-generation ground-based detectors will observe approximately  $10^5$  times the volume of current detectors. If reverse coupling events exist at rates consistent with PBH abundance constraints, these instruments should detect hundreds to thousands of events, enabling statistical tests of the polarization-mass-ratio scaling law.



## 8. Discussion

### 8.1 From Interpretive Architecture to Geometric Coupling Theory

This paper is the first entry in the Geometric Coupling Theory (GCT) programme, which extends the Interpretive Architecture (IA) corpus — a closed body of 24 papers developing a pre-formal structural layer for understanding coupling dynamics across substrates. The IA corpus built the framework: Basin Architecture, the Mechanical Spine, Flat-Region dynamics, Measurement Substrate Relativity. GCT uses that framework to generate testable predictions in specific physical domains.

The reverse coupling geometry explored here is a direct application of IA's Basin Architecture: the system transitions between attractor basins (unbound  $\rightarrow$  bound) via a saddle crossing, with the transition dynamics determined by the basin topology rather than local perturbation. The observation that asymmetry is the feature — that the polarization of the burst encodes the mass ratio — is a specific case of Measurement Substrate Relativity (Dunn, 2026): the same physical event produces different classified outcomes depending on the measurement substrate. Here, the measurement substrate is the detector orientation, and the classified outcome is the observed  $h^+/h^\times$  ratio.

The IA corpus is the lens. Geometric Coupling Theory is what the lens reveals when pointed at specific systems. This paper points it at primordial black hole dynamics. Future GCT papers will point it at neural network training dynamics, governance coupling failures, and the formalization targets identified in the IA corpus.

### 8.2 Limitations

This paper uses a simplified EOB framework at 2PN order. Higher-order post-Newtonian corrections, particularly the spin-orbit terms at 2.5PN and 3.5PN, may modify the barrier structure and the precise waveform shape. Full numerical relativity simulations would provide definitive waveforms for comparison.

The radiation reaction is included at leading order only. For the burst-like events considered here — where the waveform is concentrated in a few orbital periods near closest approach — this is a reasonable approximation, but higher-order dissipative effects could modify the tail of the burst.

The fragmentation hypothesis (suggesting that reverse coupling events could produce dark matter fragments) is not developed in this paper. It requires separate treatment with a defensible physical mechanism and is reserved for future work.

## 9. Conclusion

Reverse coupling of primordial black holes with anti-aligned spins produces a gravitational wave burst that is qualitatively distinct from chirp signals. The burst arises from two convergent mechanisms — barrier snap and geometric capture — both terminating in asymmetric accretion of the subordinate mass by the dominant mass.

The core prediction is that the burst polarization asymmetry encodes the mass ratio. Numerical simulation at three mass ratios confirms this, and a full viewing-angle sweep separates the intrinsic mass-ratio signal from observation geometry. The analytic scaling law  $h_{\times}/h_{+} \propto v/(1+q)^{1/2}$  matches the numerical results.

The prediction is falsifiable. The waveform templates are provided for injection into existing LIGO burst search pipelines. Detection would reveal a new class of gravitational wave source. Non-detection constrains the primordial black hole population and reverse coupling cross-section.

Asymmetry is the observable. The universe is asymmetrical. It is a feature, not a flaw.

## Acknowledgments

Computational derivations were developed in collaboration with large language model systems (DeepSeek, Claude) serving as domain-specific reasoning tools within a multi-model research pipeline. The theoretical framework, physical intuitions, spatial geometry, and interpretive architecture are solely the author's. The simulation code was implemented and executed by Claude; the EOB Hamiltonian formulation and analytic scaling law derivation were developed with DeepSeek. The author is responsible for all claims and any errors.

This paper inaugurates the Geometric Coupling Theory programme, extending the Interpretive Architecture corpus (24 papers, Zenodo) into domain-specific testable predictions. The complete IA corpus is available on Zenodo under the author's profile.

## References

- [1] Buonanno, A. & Damour, T. (1999). Effective one-body approach to general relativistic two-body dynamics. *Physical Review D*, 59(8), 084006.
- [2] Damour, T. (2001). Coalescence of two spinning black holes: an effective one-body approach. *Physical Review D*, 64(12), 124013.
- [3] Campanelli, M., Lousto, C.O., Zlochower, Y., et al. (2006). Gravitational radiation from merging binary black holes. *Physical Review D*, 73(6), 061501.
- [4] Kesden, M. (2012). Can binary mergers produce maximally spinning black holes? *Physical Review D*, 85(2), 024037.
- [5] Abbott, B.P. et al. [LIGO Scientific and Virgo Collaborations] (2016). Observation of gravitational waves from a binary black hole merger. *Physical Review Letters*, 116(6), 061102.
- [6] Carr, B., Kühnel, F., & Sandstad, M. (2016). Primordial black holes as dark matter. *Physical Review D*, 94(8), 083504.
- [7] Klimentenko, S. et al. (2016). Method for detection and reconstruction of gravitational wave transients with networks of advanced detectors. *Physical Review D*, 93(4), 042004.
- [8] Dunn, J.E. (2025–2026). Interpretive Architecture corpus (24 papers). Zenodo. [https://zenodo.org/search?q=metadata.creators.person\\_or\\_org.name%3A%22Dunn%2C+James+E.%22](https://zenodo.org/search?q=metadata.creators.person_or_org.name%3A%22Dunn%2C+James+E.%22)
- [9] Dunn, J.E. (2026). Coupling Outcomes Across Measurement Substrates. Unpublished manuscript.
- [10] Dunn, J.E. (2025). Approach Geometry and Deterministic Basin Dynamics Near the Half-Collinear Boundary. Zenodo. <https://doi.org/10.5281/zenodo.18727570>
- [11] Dunn, J.E. (2025). Basin Architecture at Cosmological Scale. Zenodo. <https://doi.org/10.5281/zenodo.18905846>